
Amorphous phase formation in plasma-sprayed hydroxyapatite coatings

K. A. Gross, C. C. Berndt, H. Herman

Thermal Spray Laboratory, Department of Materials Science and Engineering, State University of New York at Stony Brook, Stony Brook, Nezu York

Received 4 October 1995; accepted 12 March 1997

Abstract: The amorphous phase content of air plasma-sprayed hydroxyapatite coatings is dependent upon spraying and deposition conditions. X-ray diffraction and optical microscopy were used to investigate the influence of spray parameters on the formation of the amorphous phase. Results show three factors which most influence the formation of the amorphous phase: dehydroxylation of the molten particle during flight, the cooling rate as it impinges onto the metal substrate, and the substrate temperature. Crystalline regions were identified as unmelted particles and elongated recrystallized areas. Amorphous phase regions vary

throughout the coating but are more commonly found at the coating-substrate interface, i.e., the regions decrease toward the surface of the coating. Such an inhomogeneous distribution of phase content is expected to affect the clinical process of bone deposition, and therefore successful implant fixation. © 1998 John Wiley & Sons, Inc. *J Biomed Mater Res*, **39**, 407414, 1998.

Key words: plasma spraying; amorphous phases; hydroxyapatite; coating microstructure; X-ray diffraction

INTRODUCTION

Hydroxyapatite coatings have received a mixed reaction within the orthopedic and dental communities.¹ The variability in success of hydroxyapatite coatings has caused the U.S. Food and Drug Agency to place tighter restrictions on the requirements for hydroxyapatite coatings. This is in part due to coating vendors producing coatings ranging from 25 to 200 μm ,²⁻⁴ but more important, with different amounts of the amorphous phase.⁵⁻⁷

Atmospheric plasma spraying is becoming the main process of the thermal spray methods and is commonly used to apply hydroxyapatite to dental implants and orthopedic prostheses. Powder is injected into the plasma flame and accelerated to about 200 m/s before impacting the substrate.^{8,9} These high-impact velocities supply kinetic energy which is expended in spreading the molten droplet and creating lamellae with a large surface area. The large contact area with the substrate associated with the lamellae facilitates rapid heat transfer which may be sufficient

to form the amorphous phase. The rapid solidification arising from the high cooling rates in plasma spraying has produced amorphous phases from pure ceramics such as alumina,¹⁰ eutectic compositions of ceramic components such as alumina-zirconia,¹¹ and iron based alloys¹² or cobalt-tungsten-carbon.¹³

Various intrinsic factors could be responsible for the formation of the amorphous phase. The two most important factors which determine the glass forming abilities of a material are the viscosity and the increase in viscosity with decreasing temperature.¹⁴ The phase diagram $\text{CaO-P}_2\text{O}_5$ exhibits numerous eutectic points,¹⁵ one of which lies very close to the composition of hydroxyapatite. This infers that the cooling of a hydroxyapatite melt produces a "liquidus temperature effect" enabling the liquid to cool to lower temperatures before solidification, and increasing the likelihood of producing an amorphous phase. The glass formation tendency is further accentuated by the composition and complexity of the crystal structure of hydroxyapatite. Phosphate tetrahedra are glass formers and the large entropy of fusion, and difference in atomic arrangements between the corresponding crystalline state^{16,17} could accentuate the glass-forming ability of hydroxyapatite. Finally, crystallization to an intricate structure requires more time for diffusion of the atoms or groups to lattice sites. Plasma spraying of the superconductor material $\text{YBa}_2\text{Cu}_3\text{O}_{7-x}$,

Correspondence to: K. Gross, Department of Materials Science, University of Technology, Sydney, Box 123, Broadway NSW 2007, Australia

which also has a complex structure, has shown that it is very likely to form an amorphous phase upon plasma spraying.¹⁸ Despite these intrinsic factors, the processing conditions play a role in determining the amorphous phase content of hydroxyapatite coatings. This article addresses the influence of processing conditions on the formation of the amorphous phase.

Crystallinity has been interpreted in different ways within the biomedical community. It was initially used as an indication of the crystal size or perfection of the crystal lattice in hydroxyapatite crystals.¹⁹ Thermally sprayed materials typically have a fine grain size and high defect contents due to the fast cooling rate. These features, in addition to residual stresses, result in a broadening of the X-ray diffraction peaks, comparable to the spectrum of the inorganic phase in bone (Fig. 1). A high-crystallinity hydroxyapatite material is included as a reference. The focus of the present article is the amorphous phase represented by the broad diffuse peak in the X-ray diffraction pattern (e.g., Fig. 1, curve c). An understanding of the formation of the amorphous phases and their location within the coating is necessary to manufacture coatings that exhibit desired properties.

MATERIALS AND METHODS

Coating preparation

A Metco 3MB plasma spray torch with a GH nozzle was used to prepare hydroxyapatite coatings. Powder with a Ca/P ratio of 1.67 and impurities measured as 0.44 wt % Mg, 0.008 wt % Na, and 0.02 wt % F was supplied by Osteonics. The particle size distribution of 540 μm was used for plasma spraying unless specified. Powder was injected external to the gun and perpendicular to the plasma flow.

The powder was sprayed at different power levels to investigate the effect of processing conditions on amorphicity. The parameters that were changed include stand-off distance (5–20 cm), particle size distribution (the small particle sized powder was mixed with a larger particle size powder with a mean of 80 μm), substrate angle (0° – 60°), primary gas flow rate (90–110 lpm), air cooling of the coating and substrate during spraying, and hydroxylation state of the starting powder. A powder with a lower hydroxyl content was produced by heating at 1200°C for 1 h, followed by sieving. A substrate angle of 90° represents a substrate with the face positioned perpendicular to the stream of molten droplets. Prior to spraying, substrates were grit blasted with 150 μm SiC powder.

Calibration of amorphicity using X-ray diffraction

The as-received amorphous coating was ground in a mortar and pestle to obtain a small particle size. The crystalline commercial powder, supplied by Osteonics, was used to represent a 100% crystalline sample. Weight fractions of the

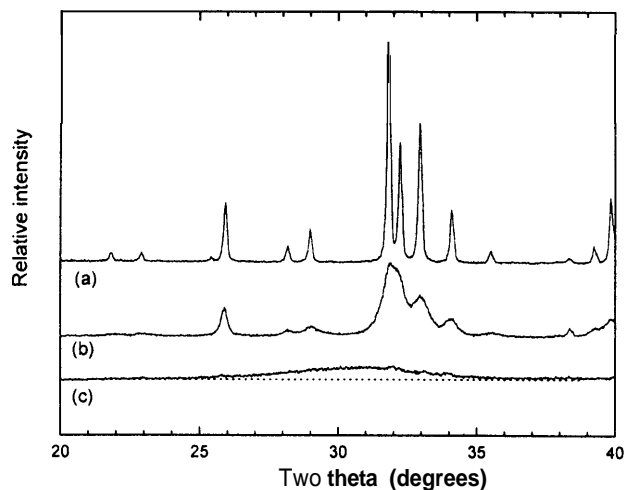


Figure 1. An X-ray diffraction pattern illustrating (a) high crystallinity hydroxyapatite, (b) inorganic bone, and (c) an amorphous phase found in hydroxyapatite coatings.

amorphous powder and the crystalline powder were mixed in increments of 10 wt % and analyzed in a flat-plate geometry with X-ray diffraction (using $\text{Cu K}\alpha$ radiation of $\lambda = 1.54 \text{ \AA}$). The X-ray diffraction goniometer was set at a scan rate of $0.01^\circ/\text{s}$, and a counting time of 2 s was used. A curve of best fit to the diffuse peak was drawn to represent the amorphous phase. The hydroxyapatite peaks were identified using JPDS card 9-432 in the 2θ range of 20° – 40° . The crystalline peak area (I_c) and the amorphous area (I_a) determined as a rise from the background (Fig. 1, curve c) were measured, and I_c/I_a was then calculated, where $I = I_c + I_a$. Therefore, an empirical calibration curve (Fig. 2) could be used to precisely (± 3 wt %) quantify the amorphous phase within thermal spray coatings. This procedure is similar to calibration curves produced by Flach et al.²⁰ and Keller et al.²¹

Coating analysis

Coatings were sectioned on a diamond cut-off wheel, mounted in epoxy resin, ground and polished using 0.05 μm

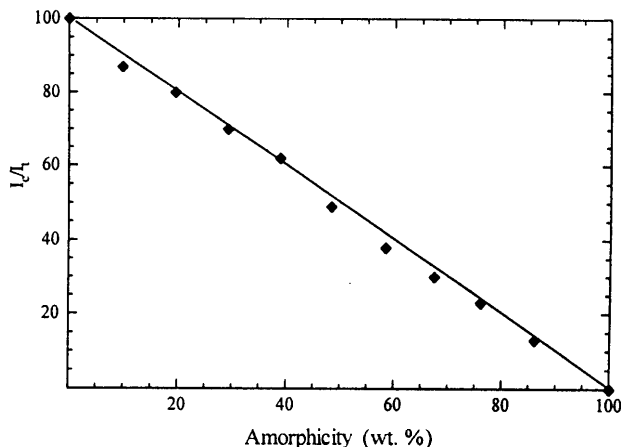


Figure 2. Calibration curve showing I_c/I_a versus amorphicity for normalized areas determined by X-ray diffraction.

alumina. The crystalline regions were viewed in the optical microscope using the Nomarski interference method to increase the depth of field and contrast of the features.

Two coatings with 98 wt % amorphous phase were heated to 660°C for 5 min in either dry or moist helium gas. The crystallinity was then measured using X-ray diffraction to ascertain the influence of the water content on the crystallization.

RESULTS AND DISCUSSION

Amorphous phase formation is linked to various stages of the plasma-spraying process: (a) interaction of the particles with the plasma, (b) spreading of the droplet on the substrate (i.e., cooling rate), and (c) temperature of the surface onto which the droplet flattens. The influence of these stages on the final coating amorphous content will be discussed.

Cooling-rate controlled amorphicity

A study of coatings produced under varying conditions provides insight into the factors responsible for the amorphous phase. As the spray angle deviates from perpendicular to the substrate by more than 30°, an increase in amorphicity is noted (Fig. 3). Less partially unmelted particles participate in the buildup of the coating as they ricochet from the surface, but more important, the lamellae thickness decreases, as evidenced from studies of other materials.²² This leads to a higher cooling rate and is associated with an increase in amorphicity. The primary plasma gas flow rate also influences the amount of amorphous phase formed. A higher primary gas flow rate transfers more velocity to the particle before impact. Greater particle flattening produces a higher cooling rate.

The viscosity of the melt can be decreased by heating the molten particles to a higher temperature. This has been demonstrated by Wolke et al.,²³ in whose study a higher enthalpy plasma flame was employed. Overheating, however, will cause decomposition first to tricalcium phosphate and tetracalcium phosphate and then to calcium oxide and more tetracalcium phosphate. For a given droplet size, the lower viscosity aids spreading of the melt to produce a thinner lamella. The spreading of the droplet on the substrate giving rise to the amorphous phase in hydroxyapatite coatings produces good substrate contact which can increase the interfacial adhesion bond strength of the coating.²⁴

The nature of the substrate and successively deposited layers also play a role in droplet spreading and, hence, the cooling rate.²⁵ The first molten droplets impact the titanium surface, which may become oxidized

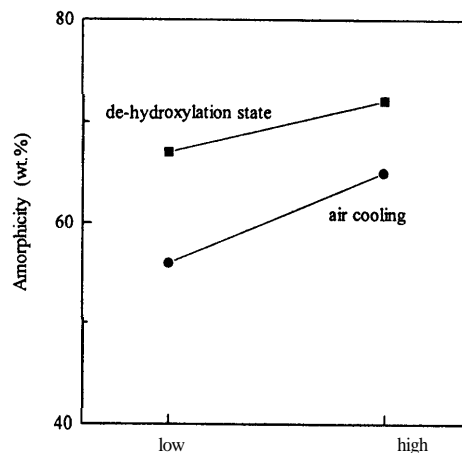
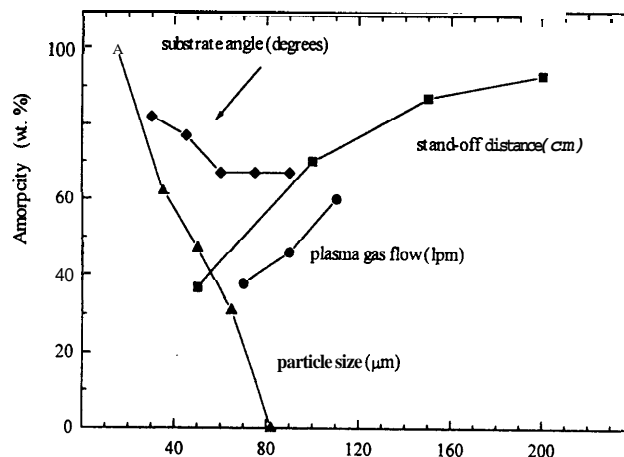


Figure 3. Influence of spray parameters on the amorphicity of the coating. Abscissa is variable according to values or level of parameter. Amorphous content was determined by X-ray diffraction.

during the preheat stage. Oxide layers on metal substrates present a thermal contact resistance to the molten droplet and can alter the microstructure of the lamellae.²⁶ However, the cooling rate on the very thin film of oxidized titanium is sufficiently fast to produce an amorphous phase. Furthermore, this thin oxide layer is important for bonding of the coating to the substrate.²⁷

The cooling rate can also be modified by the substrate roughness which determines coating quality.²⁸ A rough substrate prevents spreading of the droplet, thus lowering the cooling rate. As the coating is manufactured, successive layers will also present a rough surface and prevent spreading of a liquid droplet. Therefore, crystalline areas may be larger and randomly placed in the coating. It will be shown in the following section how splashing of liquid with a com-

position of hydroxyapatite produces satellite droplets, resulting in small crystalline regions.

The first molten droplets will dissipate heat to the titanium substrate and cool at a rate of approximately 10^5 K/s,²⁹ producing an amorphous material adjacent to the substrate. Heat flow to the substrate will be higher than to the surrounding air; however, convection cooling of the coating can be employed as an additional means of increasing the cooling rate.

Composition-controlled amorphicity

Amorphicity can be controlled by varying other process parameters or the original feedstock (Fig. 3). The first parameter that was recognized as producing a larger level of amorphicity was the stand-off distance (i.e., the distance between the particle injection point and the object to be coated).^{30,31} A larger stand-off distance will produce thicker splats, yielding an overall lower cooling rate of the splat but a higher level of amorphicity. The longer time at the elevated temperature produces more dehydroxylation, which influences the formation of the crystalline phase. The shape of the curve (Fig. 3) (proportional to $t^{1/2}$) is representative of diffusion from the surface of a sphere.³²

The particle size of the powder also affects the formation of the amorphous phase. A smaller particle size permits higher heat transfer and more complete hydroxyl ion diffusion from the surface of in-flight molten particles. A narrow particle size distribution will permit more control over the particle temperature history and lead to more predictable dehydroxylation and higher uniformity throughout the coating. The effect of dehydroxylation seems to have a greater influence in comparison to the increase in the cooling rate.

Removal of hydroxyl ions can be performed before spraying by using a dehydroxylated powder. This increases the amount of amorphous phase in the coating (Fig. 3). The heat of the plasma is then directed to further lowering the hydroxyl concentration of the traveling particles. Weng et al.³³ observed an increasing amorphicity with powders of a lower hydroxyl content but variable porosity.³⁴ The porosity affects the thermal diffusivity, and this makes it difficult to determine the main cause leading to changes in the amorphous phase content. Calcination at higher temperatures concomitantly reduces the porosity and the hydroxyl content, which affects the thermal diffusivity and further dehydroxylation during spraying. Thus, a hydroxyl deficient feedstock material will more likely give rise to an amorphous phase compared to a high hydroxyl content powder.

A model presented by Khor and Cheang,³⁵ in which the outside skin of a particle is molten and the core is unmolten, depicts only one possibility where insufficient heat is transferred to completely melt the particle. This model must be modified by assuming that the particle is totally molten with a hydroxyl rich core (depicting the stoichiometry of hydroxyapatite) and a hydroxyl-depleted skin. Formation of the amorphous phase can be attributed to many factors and will be discussed from a kinetics and thermodynamics perspective.

Mechanistically, the number of anions (O^{2-} /unit cell) participating in the diffusion process in oxyapatite (i.e., a completely dehydroxylated hydroxyapatite) is considerably less compared to hydroxyapatite where the hydroxyl ions are twice in number ($2OH^-$ /unit cell) and more mobile, owing to the lower charge state. The necessary atomic restructuring to an apatitic crystal structure is thus easier for a hydroxylated melt. This is assisted by a lower melt viscosity found in calcium phosphates with a higher "water content."³⁶ A dehydroxylated molten particle will thus have a higher nucleation barrier for crystallization.

A thermodynamic approach to crystallization requires consideration of the Gibbs free energy of formation (Fig. 4). The free energy of formation is larger for hydroxyapatite than oxyapatite,^{37,38} and hence, the driving force for nucleation of hydroxyapatite is higher. The hydroxyl-depleted area is thus more sensitive to the cooling rate and remains as an amorphous phase under rapid cooling conditions.

The crystallization of hydroxyapatite may also depend upon coating impurities. For example, a divalent cation such as magnesium can replace calcium. Magnesium has a smaller atomic radius and is more

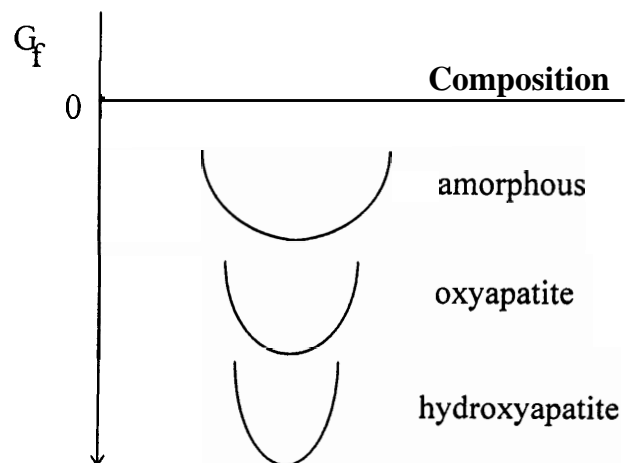


Figure 4. Free energy of formation of oxyapatite and hydroxyapatite compared to the amorphous phase (schematic only).

strongly bound to the phosphate groups than is the calcium ion.³⁹ This stronger bonding forms a more stable configuration which could hinder crystallization by forming a diffusion barrier. Similarly, the anions can also be replaced, but this will lead to an opposite effect. A substitution of fluorine for hydroxyl ions will provide a higher driving force for crystallization to fluorapatite. The composition should thus be considered in conjunction with cooling, since a melt with a higher driving force for crystallization will need a higher cooling rate to form an amorphous phase.

Crystallization during coating build-up

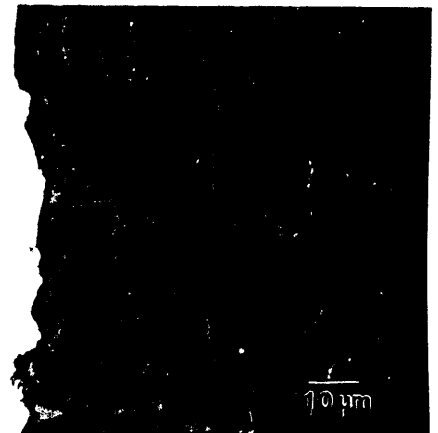
Measurement of the amorphous phase content at the coating surface by conventional X-ray diffraction is not representative of the average amorphous phase content of the coating. The amorphous region in the coating microstructure is distinguished from the crystalline area by its ease of removal in the polishing stage of specimen preparation. Figure 5 shows the microstructure of 50 wt % and 100 wt % crystalline coatings determined by X-ray diffraction. A noteworthy feature is the amorphous phase (darker gray) which very often forms at the titanium substrate. This is important in the performance of the coating, since dissolution of this layer adjacent to the substrate could lead to failure. Other phases may be present in small quantities; however, these cannot be distinguished from the hydroxyapatite.

The crystalline phase consists of unmolten or partially molten particles and recrystallized regions. The unmolten particles, not having experienced full heat transfer, are transferred to the coating with a morphology representative of the starting powder. Molten droplets participate in coating build-up but do not always form a splat of even thickness. Thicker sections are accompanied with a lower cooling rate and can produce sites of crystallization. These latter crystalline regions will be small in size (Fig. 6), but will grow under thermal activation provided by the heat transfer of subsequent deposited layers. The detection of the crystalline regions may not always be simple. The amorphous phase appears transparent, but this optical property has also been observed for crystalline hydroxyapatite which has been hydroxide depleted.⁴⁰

Heat treatment of an amorphous phase in a dry and wet gas shows that the latter gives rise to a more extensive crystallization (Fig. 7). During the deposition process, the molten particle, with a hydroxyl rich core surrounded by a hydroxyl deficient region, spreads out to form the lamellae. The individual lamellae can-



(a)



(b)

Figure 5. Microstructures showing the crystalline phase (indicated by higher plateaus of lighter color) in (a) a 50 wt % and (b) a 100 wt % crystalline coating calculated from X-ray diffraction. The titanium substrate is situated on the left-hand side and the spray direction is indicated by the arrow.

not be distinguished in hydroxyapatite coatings; however, it is expected that the hydroxyl-rich region is more likely to form the crystalline phase. The crystalline phase that forms upon deposition will appear as elongated particles (Figs. 5 and 8). These two regions are inseparable if the cooling rate is sufficiently rapid, and both will constitute the amorphous phase. The fast cooling rate of the first lamellae is controlled by the rapid heat dissipation to the titanium substrate (thermal diffusivity of titanium is $8 \times 10^{-2} \text{ cm}^2/\text{s}$). This may be modified if the titanium has been oxidized significantly before the deposition stage. Further dissipation is hindered by the low thermal conductivity of the successive layers.

The heat in the coating is delivered by molten particles impinging on the coating. Heat is dissipated slowly owing to the low thermal diffusivity of hydroxyapatite ($\sim 5 \times 10^{-3} \text{ cm}^2/\text{s}$)⁴¹ and is elevated by released heat owing to the structural relaxation of the amorphous phase and the recalescence of the crystal-

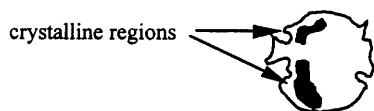


Figure 6. Crystalline region identified by light microscopy in a splat. Arrows indicate crystalline areas within the flattened particle.

lizing areas. Thermal conductivity of the coating is affected by the amorphous phase and pore content. An amorphous phase has typically a lower thermal conductivity—i.e., a sixfold difference at 200°C between silica and quartz.⁴² The amorphous phase formed in hydroxyapatite coatings will thus give rise to a faster rise in temperature during coating deposition. When the temperature is sufficiently high, recrystallization will first take place in the hydroxyl-rich area. The elongated crystalline regions, if not formed during solidification, must then be recrystallized areas. Recrystallization will occur more readily on den-

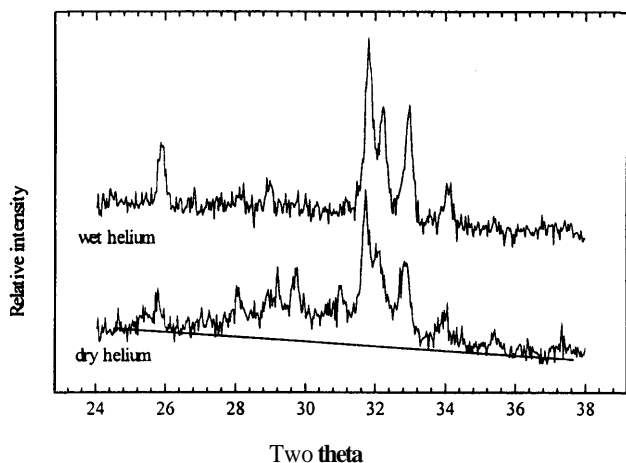
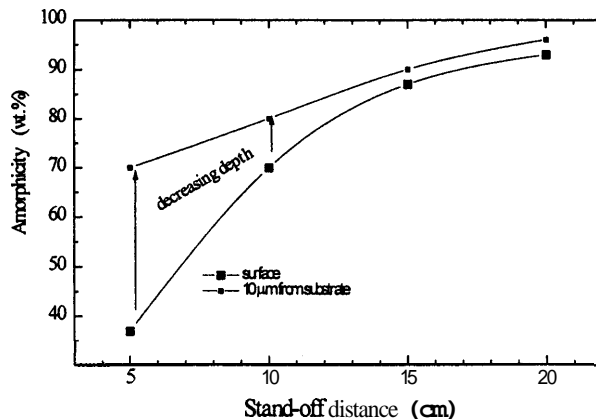
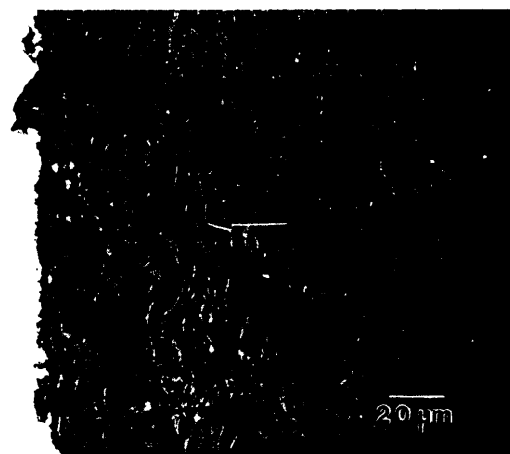


Figure 7. X-ray diffraction of the amorphous phase after heat treatment at 660°C for 5 min in a dry and moist atmosphere.



(a)



(b)

Figure 8. The variation of crystallinity close to the substrate and on the surface of the coating as (a) identified by X-ray diffraction and (b) shown in a micrograph sprayed at 10 cm stand-off distance.

tal implants of lower thermal mass compared to hip implants.

As consecutive layers are deposited, the heat in the coating builds up slowly and leads to crystallization in different places within the coating. The coating is thus more crystalline at the surface compared to the area adjacent to the substrate (Fig. 8). This has also been observed by Le Geros.⁴³ The heat build-up also arises owing to pores within the coating material. Pores are intrinsic to thermal spray coatings and can decrease the thermal diffusivity by a factor of five when oriented parallel to the surface.⁴⁴ McPherson⁴⁵ showed that the thermal conductivity of alumina decreases by at least an order of magnitude, and modeling by Hollis⁴⁶ suggested that this is also dependent on the size and distribution of the elongated pores between the lamellae. Ilavsky et al.⁴⁷ recently addressed the influence of spraying parameters and found an influence of

spray angle on crack orientation within lamellae. These cracks form as a result of the shrinkage produced in the crystallization process.²⁹ The number of crystalline regions identified as recrystallized hydroxyapatite thus increases with thickness owing to the intrinsic low thermal diffusivity, and is furthermore accentuated by the amorphous phase and coating porosity.

This investigation has illustrated how coating crystallinity can be altered by changes in the process and deposition stage. By ensuring low dehydroxylation, coatings with a high crystalline content can be produced with the intention of a longer lifetime. Understanding the amorphous phase formation and the ability to examine microstructures will aid in decreasing the variability in hydroxyapatite coatings leading to a better *in vivo* performance predictability.

CONCLUSIONS

Hydroxyapatite has two intrinsic properties that enable it to form an amorphous phase. First, it is made up of phosphates which are glass formers, and second, the composition of hydroxyapatite is very close to the eutectic composition, thus inducing a liquidus effect. Thermal spraying produces the amorphous phase, not only due to the high cooling rate but also to the removal of hydroxyl ions which make it more difficult for the crystalline phase to form. The hydroxide content can be controlled with processing parameters or, alternatively, at the powder-processing stage.

Optical microscopy is a useful tool for discerning crystalline regions. The crystalline phase consists of unmolten and recrystallized areas within the coating. Recrystallization during coating production takes place preferentially in the hydroxyl-rich regions of the amorphous phase.

The authors are grateful for the translations of articles from Russian by Mrs. Maija Ambrena of the Engineering Planning and Network Office, "Karlis," Latvia.

References

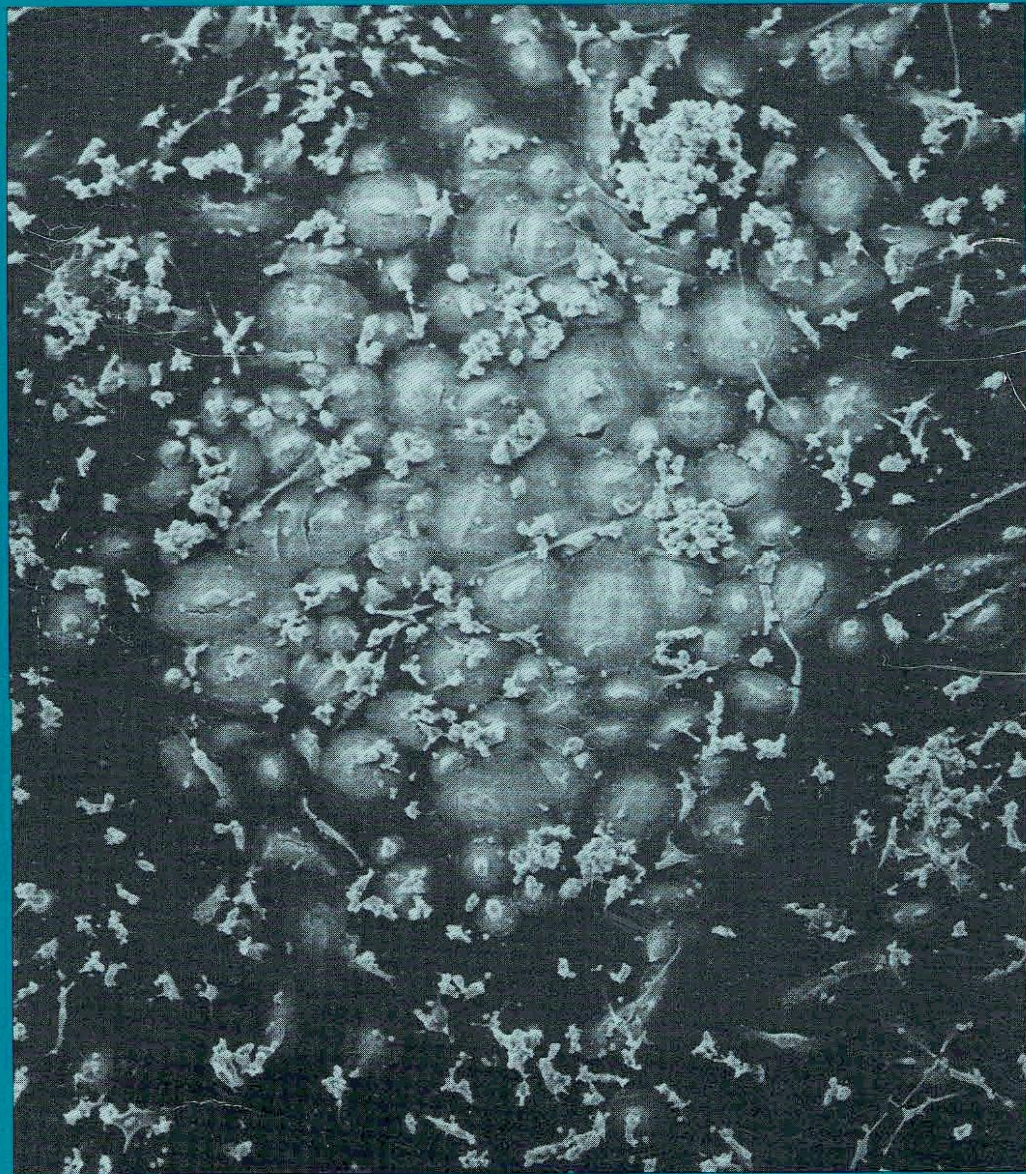
1. S. D. Cook, T. Albrektsson, R. A. Yukna, and G. de Lange, "Current issues forum: What is your opinion concerning the long-term consequences of HA coatings within bone," *Int. J. Oral Maxillofac. Implants*, **7**, 302–310 (1992).
2. R. G. T. Geesink, "Five year results of hydroxyapatite-coated total hip replacement," *J. Bone Joint Surg.*, **75B(Suppl. II)**, 127 (1993).
3. C. Nourissat, J. Adrey, D. Berteaux, C. Goaland, A. Gueret, and G. Hamon, "Hydroxyapatite and bone ingrowth—myth or reality? Analysis of results at 4 years in the ABG hip prosthesis," *J. Bone Joint Surg.*, **75B(Suppl. II)**, 127 (1993).
4. J. Karrholm, H. Malchau, F. Snorrason, and P. Herberts, "Micromotion of femoral stems in total hip arthroplasty—a randomized study of cemented, hydroxyapatite-coated, and porous coated stems with roentgen stereophoto-grammetric analysis," *J. Bone Joint Surg.*, **76A**, 1692–1705 (1994).
5. J. T. Krauser, "X-ray diffraction analysis of hydroxyapatite-coated implants," in Abstracts from the 7th Annual Meeting of the Academy of Osseointegration, Vancouver, British Columbia, Canada, February 27–29, 1992.
6. P. Glick, K. Versman, and D. Allen, "X-ray diffraction comparison of hydroxyapatite coated dental implants," in Abstracts from the 7th Annual Meeting of the Academy of Osseointegration, Vancouver, British Columbia, Canada, February 27–29, 1992.
7. P.-O. Kroon and M. A. R. Freeman, "Hydroxyapatite coating of hip prosthesis. Effect of migration into the femur," *J. Bone Joint Surg.*, **74B**, 518–522 (1992).
8. P. Fauchias, J. F. Coudert, M. Vardelle, A. Vardelle, and A. Denoirjean, "Diagnostics of thermal spray plasma jets," *J. Thermal Spray Technol.*, **1**, 117–128 (1992).
9. E. Pfender, "Plasma jet behavior and modeling associated with the plasma spray process," *Thin Solid Films*, **238**, 228–241 (1994).
10. G. Tremouilles, J. L. Derep, and R. Portier, "Plasma-coated metal-zirconia interface," in *Advances in Thermal Spraying*, Pergamon Press, New York, 1986, pp. 445–454.
11. N. Claussen, G. Lindemann, and G. Petzow, "Rapid solidification in the Al_2O_3 - ZrO_2 system," *Ceram. Int.*, **9**, 83–86, (1983).
12. T. P. Shmyreva and L. V. Mukhina, "Formation behaviour of new amorphous and composite materials in detonation gun and plasma spraying," in *Thermal Spray Industrial Applications*, C. C. Berndt and S. Sampath (eds.), ASM International, Materials Park, OH, 1994, pp. 201–204.
13. J. Nerz, B. Kushner, and A. Rotolico, "Microstructural evaluation of tungsten carbide-cobalt coatings," *J. Thermal Spray Technol.*, **1**, 147–152 (1992).
14. D. R. Uhlmann, "A kinetic study of glass formation," *J. Non-cyst. Solids*, **7**, 337–348 (1972).
15. P. V. Riboud, "Composition and stability of apatites in the system CaO - P_2O_5 -iron oxide- H_2O at high temperature," *Ann. Chim.*, **8**, 381–390 (1973).
16. W. H. Zachariassen, "The atomic arrangement in glass," *J. Am. Chem. Soc.*, **54**, 3841–3851 (1932).
17. L. D. Pye, H. J. Stevens, and W. C. La Course (eds.), *Introduction to Glass Science*, Plenum Press, New York, 1972.
18. R. Neiser, "Structure-processing-property relationships in air plasma sprayed $YBa_2Cu_3O_{7-x}$," PhD dissertation, SUNY Stony Brook, Stony Brook, New York, 1989.
19. R. Le Geros, "Biodegradation and bioresorption of calcium phosphate ceramics," *Clin. Mater.*, **14**, 65–88 (1993).
20. J. S. Flach, L. A. Shimp, C. A. van Blitterwijk, and K. de Groot, "A calibrated method for crystallinity determination of hydroxyapatite coatings," in *Characterization and Performance of Calcium Phosphate Coatings for Implants*, ASTM STP 1196, E. Horowitz and J. E. Parr (eds.), American Society for Testing and Materials, Philadelphia, 1994, pp. 25–32.
21. L. Keller and P. Rey-Fessler, "Non-destructive characterization of hydroxyapatite coated dental implants by XRD method," in *Characterization and Performance of Calcium Phosphate Coatings for Implants*, ASTM STP 1196, E. Horowitz and J. E. Parr (eds.), American Society for Testing and Materials, Philadelphia, 1994, pp. 54–62.
22. G. Montavon, S. Sampath, C. C. Berndt, H. Herman, and C. Coddet, "Effects of vacuum plasma spray processing parameters on splat morphology," *J. Thermal Spray Technol.*, **4**, 67–74 (1995).
23. J. G. C. Wolke, C. P. A. T. Klein, and K. de Groot, "Bioceramics for maxillofacial applications," in *Bioceramics and the Human*

- Body, A. Ravaglioli and A. Krajewski (eds.), Elsevier Science Publishers, Amsterdam, 1991, pp. 166–180.
24. F. Brossa, A. Cigada, R. Chiesa, L. Paracchini, and C. Consonni, "Post-deposition treatment effects on hydroxyapatite vacuum plasma spray coatings," *Biomaterials*, 5, 855–857 (1994).
 25. P. Fauchais, M. Vardelle, A. Vardelle, L. Bianchi, and A. C. Leger, "Parameters controlling the generation and properties of plasma sprayed zirconia coatings," *Plasma Chem. Plasma Proc.*, 16, 99S–126S (1996).
 26. M. Pasandideh-Fard and J. Mostaghimi, "On the spreading and solidification of molten particles in a plasma spray process: Effect of thermal contact resistance," *Plasma Chem. Plasma Proc.*, 16, 83S–98S (1996).
 27. K. de Groot, "Hydroxylapatite as coating for implants," *Inter-ceram*, 4, 38–41 (1987).
 28. S. J. Yankee, B. J. Pletka, and R. L. Salsbury, "Quality control of hydroxylapatite coatings: The surface preparation stage," in *Thermal Spray Coatings: Properties, Processes and Applications*, T. F. Bernecki (ed.), ASM International, Materials Park, OH, 1991, pp. 475–480.
 29. K. A. Gross, "The amorphous phases in hydroxyapatite coatings," PhD dissertation, SUNY Stony Brook, Stony Brook, New York, 1995.
 30. H. Ishimaru and H. Oonishi, "Characterization of the material properties of the plasma spray coated hydroxyapatite," in *Bio-ceramics 2*, Deutsche Keramische Gesellschaft e. V., Koln, 1990, pp. 219–226.
 31. K. A. Gross and C. C. Berndt, "Optimization of spraying parameters for hydroxyapatite," in *2nd Plasma-Technik Symposium*, Vol. 3., S. Blum-Sandmeier, H. Eschnauer, P. Huber, and A. R. Nicoll (eds.), Hafflinger Druck AG, Wettingen, 1991, pp. 159–170.
 32. J. Crank, *The Mathematics of Diffusion*, 2nd ed., Clarendon Press, Oxford, 1975.
 33. J. Weng, X.-G. Liu, X.-D. Li, and X.-D. Zhang, "Intrinsic factors of apatite influencing its amorphization during plasma-spray coating," *Biomaterials*, 16, 39–44 (1995).
 34. X. Zhang, J. Chen, J. Zhou, J. Feng, and C. Li, "Porous hydroxyapatite granules: Their synthesis, application and characterisation," *Clin. Mater.*, 4, 319–327 (1989).
 35. K. A. Khor and P. Cheang, "Characterization of plasma sprayed hydroxyapatite powders and coatings," in *Thermal Spray Coatings: Research, Design and Applications*, C. C. Berndt and T. F. Bernecki (eds.), ASM International, Materials Park, OH, 1993, pp. 347–352.
 36. O. N. Kanchieva, N. V. Komarova, S. V. Nemilov, and D. K. Tagantsev, "Effect of water content on the viscosity of glassy sodium oxide-2-(silicon dioxide) ($\text{Na}_2\text{O} \cdot 2\text{SiO}_2$), lead oxide-2-(boron oxide) ($\text{PbO} \cdot 2\text{B}_2\text{O}_3$), and calcium oxide-phosphorus pentoxide," *Fiz. Khim. Stekla*, 6, 408–414 (1980).
 37. E. J. Duff, "Thermodynamical considerations concerning the stability of oxyapatite, $\text{Ca}_{10}\text{O}(\text{PO}_4)_6$, in aqueous media," *J. Inorg. Nucl. Chem.*, 34, 853–857 (1972).
 38. D. Williams, "Calcium phosphates and apatites" in *Concise Encyclopedia of Medical and Dental Materials*, Pergamon Press, Oxford, 1990.
 39. A. L. Boskey and A. S. Posner, "Magnesium stabilization of amorphous calcium phosphate: A kinetic study," *Mater. Res. Bull.*, 9, 907–916 (1974).
 40. K. Uematsu, M. Takagi, T. Honda, N. Uchida, and K. Saito, "Transparent hydroxyapatite prepared by hot isostatic pressing of filter cake," *J. Am. Ceram. Soc.*, 72, 1476–1478 (1989).
 41. T. Kijima and M. Tsutsumi, "Preparation and thermal properties of dense polycrystalline oxyhydroxyapatite," *J. Am. Ceram. Soc.*, 62, 455–460 (1979).
 42. D. R. Lide (ed.), *Handbook of Chemistry and Physics*, CRC Press, Boca Raton, FL, 1994.
 43. R. Z. Le Geros, "Calcium phosphates in oral biology and medicine," in *Monographs in Oral Sciences*, Vol. 15, H. M. Myers (ed.), Karger and Basker, New York, 1991, pp. 154–192.
 44. D. P. H. Hasselman, "Effect of cracks on thermal conductivity," *J. Composite Mater.*, 12, 403–407 (1978).
 45. R. McPherson, "A model for the thermal conductivity of plasma-sprayed ceramic coatings," *Thin Solid Films*, 112, 89–95 (1984).
 46. K. J. Hollis, "Pore phase mapping and finite-element modeling of plasma sprayed tungsten coatings," in *Thermal Spray Science and Technology*, C. C. Berndt and S. Sampath (eds.), ASM International, Materials Park, Ohio, 1995, pp. 403–409.
 47. J. Ilavsky, A. J. Allen, G. G. Long, S. Krueger, H. Herman, C. C. Berndt, and A. N. Goland, "Anisotropy of the surfaces of pores in plasma sprayed alumina deposits," in *Thermal Spraying—Current Status and Future Trends*, A. Ohmori (ed.), High Temperature Society of Japan, Osaka University, 1995, pp. 483–488.

JOURNAL OF BIOMEDICAL, MATERIALS RESEARCH

March 5, 1998
Volume 39
Number 3

AN OFFICIAL
JOURNAL OF
**THE SOCIETY FOR
BIOMATERIALS**
**THE JAPANESE
SOCIETY FOR
BIOMATERIALS**



 **WILEY**
Publishers Since 1807

ISSN: 0021-9304